DOI: 10.13009/EUCASS2025-378
11TH EUROPEAN CONFERENCE FOR AERONAUTICS AND SPACE SCIENCES (EUCASS)

Fast and Precise Calculation of Slew Durations for Agile Earth Observation Constellation Scheduling

Hermann Helgert[⋆†]*, Thomas Daubner*[⋆]*, Ramin Geshnizjani*[⋆] *and Sergio Montenegro*[‡]
[⋆]*Airbus Defence and Space GmbH*
An der B31, 88090 Immenstaad, Germany
[‡]*Julius-Maximilians-Universität Würzburg*
Emil-Fischer-Straße 70, 97074 Würzburg, Germany
hermann.helgert@airbus.com · ramin.geshnizjani@airbus.com · thomas.daubner@airbus.com
sergio.montenegro@uni-wuerzburg.de
[†]Corresponding author

Abstract

Scheduling for small Earth observation satellite constellations means to distribute tasks among the satellites and finding an optimal sequence for each individual satellite. This involves optimizing for several metrics evaluating for instance the image quality and the timeliness of delivery while respecting geometric limitations (e.g., maximum incidence angles of observations), the kinematic agility of the satellite, and the need to manage various resources like power, memory, downlink capacity and thermal load. A high density of observations on the order of several thousand per satellite per day makes this problem highly combinatorial and calls for a scalable algorithmic solution. Finding good solutions involves the precise calculation of slew durations from one observation to the next. The slew duration itself is a time dependent constraint due to the satellite's own motion and can in general not be calculated analytically. In sequences of observations, approximation errors not only add up, but due to the time dependence, any approximation gets worse with each additional step. Therefore, we propose to use a precise model and find an approximately optimal solution instead of solving an approximated model optimally. First, we provide a comprehensive formulation of the slew kinematics of agile Earth observation satellites with all relevant relations for scheduling observations. As the main contribution, we propose a parametrization for observations that allows precomputation of slew durations for the full agile satellite scheduling problem, reducing the complexity significantly. Finally, we demonstrate the application of this parametrization in a representative scenario.

1. Introduction

Agile earth observation systems (EOS) have to serve as many user requests as possible as quickly as possible with the highest possible resolution. These requirements necessitate multi-satellite systems, while at the same time the number of satellites is limited by the available budget. Getting the best performance from the EOS is therefore imperative. This is only feasible if a close to optimal scheduling routine is used.

For instance, increasing the performance of a constellation consisting of ten satellites by just over 10 % potentially allows saving construction and launch of an entire satellite. To enable this type of decision, the planning algorithm must already be considered during early mission phases as part of the overall system. Due to the iterative nature of mission performance analysis, simulating a given design – including the planner embedded in the system – must work significantly faster than real-time. Operational algorithms, on the other hand, can in principle work slower but they must solve the problem precisely or at least with sufficient fidelity and reliability to directly generate commands. During in orbit validation, the system is usually tested against scenarios established in earlier design phases. Doing this implicitly requires sufficient congruence between the operational and the algorithm used for analysis, ultimately applying both sets of requirements to each.

Even for small-scale constellations of individually highly capable satellites, the scheduling problem is complex due to the agility of the satellites and the number of user requests. To the best knowledge of the authors, there is currently no optimal solution for the full practical agile Earth observation scheduling problem. While this topic has been studied for over two decades, the solutions proposed in open literature typically require simplifying assumptions

DOI: 10.13009/EUCASS2025-378

regarding the satellites' agility (e.g., assuming only two-axis slew maneuvers or omitting the time dependency of slew durations), or imaging capability (e.g., assuming infinitely fast acquisitions).

For this reason, the first contribution of this paper is a comprehensive formulation of the general agile Earth observation scheduling problem with all requirements and constraints of current practical relevance. Based on this formulation, the gaps between the current state-of-the-art and a solution to the general problem are identified. Next, we present a fast and precise method to approximate slew durations, applicable to typical Earth observation satellites.

This paper is organized as follows: Subsection 2.1 discusses related work. In subsection 2.2, a comprehensive description of the practical problem of scheduling observations for an agile satellite is given, challenges unique to this problem are presented. Evidence for a gap between the practical problem at hand and the problems handled in various publications is shown. Section 3 introduces the derivation of the proposed method. In section 4, the application of the proposed parametrization on a scenario is shown. A direction for future work is shown in the last Section.

2. Agile Earth Observation Planning Problem

2.1 Related Work

All existing approaches to solve the satellite scheduling problem model it using graphs, where nodes can for example represent observations and edges describe relationships between them. The goal is then to select an optimal ordered set of nodes, for which there are methods available. There are classical approaches like heuristic search, dynamic programming (DP) and integer programming, and lately also machine learning. Different philosophies on the dimension in which the solution space is traversed can be seen. Some algorithms incrementally build a solution starting with an empty timeline and then working chronologically forward. Other algorithms take an existing solution and optimize it by removing and adding observations and actions with no chronological order. In the following, a brief overview is given.

2.1.1 Classical Approaches

Hall et al[6] show eight different heuristics that can be applied to guide a search algorithm. They show test results for each heuristic when applied to a graph search algorithm searching for the optimal solution. They assume a simple model, in which each request has fixed observability windows and occupies a certain duration strictly inside this window when scheduled. No other constraints are taken into account.

Others also apply a graph representation of the problem where the graph nodes represent activities and the edges represent transitions from one activity to another, encoding either the feasibility or the transition duration. Gabrel et al.[4] propose a range of graph-algorithms based on the idea of discretizing the starting times of activities, thus creating a set of possible activities with their corresponding starting time. These nodes then both appear in a conflict graph and an enchainability graph. The only constraint taken into account for the feasibility of transitions is the kinematic agility, modelled as the line-of-sight movement of the camera itself, although not considering yaw motion. The transition is assumed to be performed by changing roll and pitch independently, the slower axis then determines the overall duration. As the graph's nodes encode the corresponding start and end times and infeasible nodes are not created, the observation conditions are also taken into account. Augenstein et al.[2] then make use of a directed acyclic graph (DAG) encoding the feasibility of transitions to represent the scheduling problem for constellations instead of single satellites and also take into account additional constraints like a minimum contact frequency for every satellite. In this model, ground station contacts and data takes are mutually exclusive, since downlinks require a certain antenna pointing and can be treated equally. DP is then used to find the optimal schedule from the DAG. They heavily rely on precomputation of the mutual exclusivity between data takes, which is futile in the agile context, since the satellite is almost always able to perform any given pair of observations in one pass.

Stephenson[10] extends this concept into the agile context, encoding transition times in the nodes of the graph and connecting them according to a neural network providing transition time approximations. They show different mixed-integer programming (MIP) formulations which are then able to compute longest paths in the DAG.

The main drawback of these works is the attitude model, which does not represent the full 3-DOF problem as shown below, where the rotation about the line-of-sight and the fact that slews are generally not rest-to-rest are relevant.

Lemaître et al[8] test four different algorithms to schedule observations on short orbit arcs. Namely a greedy algorithm, a DP algorithm, a constraint programming algorithm making use of Optimization Programming Language (OPL) and finally, a local-search algorithm (LSA). The LSA starts with a feasible solution sequence. New solutions are then constructed by either removing or inserting observations. They introduce a concept similar to pheromones in the context of ant-colony-algorithms, where parameters are assigned to images, indicating the success rate of insertions. All their algorithms rely on the quick computation of transition times, which justifies the use of simplified models, but

DOI: 10.13009/EUCASS2025-378

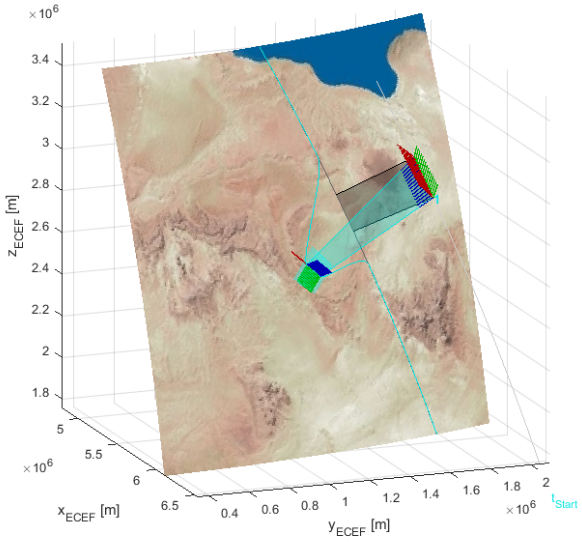

Figure 1: TDI data take

at the same time highlights the importance of computing transition times quickly and accurately. Grasset-Bourdel and Verfaillie[5] then developed a hierarchical, chronologically forward algorithm.

Aldinger and Löhr[1] present a time-discrete chronologically forward greedy approach based on Temporal Fast Downward with modules (TFD/M), focusing purely on kinematic and geometric constraints.

Nag et al[9] present a DP based optimizer intended for cube-sat constellations. Similar to some of the works shown above, the dynamics are simplified to rest-to-rest maneuvers.

2.1.2 Reinforcement Learning

Machine learning based concepts are also suggested recently, with the focus being on reinforcement learning (RL) agents. Zhao et al[14] split the problem in two, first selecting which observations to make and in which order, and then determine the specific start time of each observation. They make use of a simplified attitude model, considering only rest-to-rest maneuvers. Herrmann et al[7] formulate an EOS scheduling problem as a Markov decision process (MDP), with a high-fidelity simulation environment serving as generative state transition function. Their agent considers a planning horizon of 270 min and repeatedly plans its next actions. It can choose between taking observations with two different instruments, desaturating reactions wheels and charging the batteries. Stephenson et al[11], using the same simulation environment, also formulate the problem as MDP. They train a RL agent, varying several parameters and compare their results to their MIP-approach cited above.

2.2 Satellite Kinematics

The attitude kinematics of a satellite depend on the specific mission it carries out. In the case of agile Earth-observation missions, the satellite alternates between data takes ('scans') and reorientation maneuvers ('slews') in rapid succession. For this work, the focus is on time delay integration (TDI) type optical instruments, bit it can be readily extended to other technology. For example, staring arrays can be considered a special case of TDI with zero line rate. A target to be scanned can then be expressed as a line on the Earth's surface which the line-of-sight of the instrument must follow with some specified, generally time dependent, velocity and orientation, as for example shown in Figure 1. Planning means ordering the different scans and connecting them with slews, thereby fixing all actions in time. Therefore, the specific trajectory during the scan is not of interest. Only the start and end points of a scan are relevant, so in the pairwise consideration of scans in the scope of this work, the scans are treated as point targets, where $\boldsymbol{p}_\mathrm{t} \in \mathbb{R}^3$ describes the location on Earth's surface and $A \in [-\pi;\pi]$ describes the orientation of the target on the ground, for example with respect to local north. There must be a deterministic function f taking the target configuration $(\boldsymbol{p}_\mathrm{t}, A)$, the satellite's position $\boldsymbol{p}_\mathrm{s} \in \mathbb{R}^3$ and its velocity $\boldsymbol{v}_\mathrm{s} \in \mathbb{R}^3$ as input and giving the necessary attitude $\boldsymbol{\Psi} \in \mathrm{SO}(3)$ and angular rate $\boldsymbol{\omega}_\mathrm{s} \in \mathbb{R}^3$ of the satellite at the start and end of the scan. A function f fulfilling these requirements can usually be found analytically for both radar and optical instruments, in the following it is treated as black box to allow

DOI: 10.13009/EUCASS2025-378

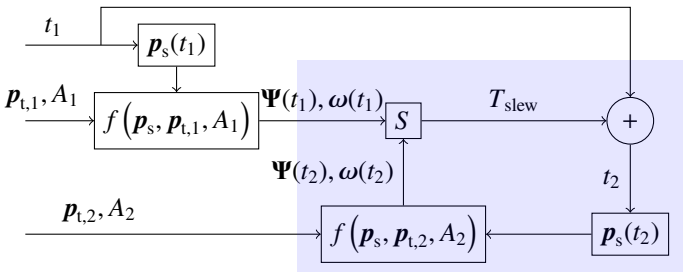

Figure 2: Iterative calculation of slew duration

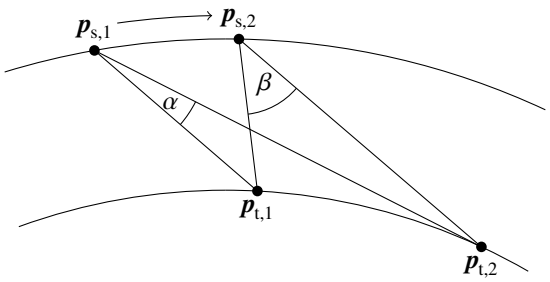

Figure 3: The apparent distance between targets from the point of view of the satellite changes

for arbitrary hardware configurations. For planning purposes, the duration of a transition T_slew from one observation to the next must be calculated, which typically involves optimizing an attitude trajectory without violation of constraints. All kinematic constraints are assumed to be constant in body-frame. They can for example be a simple box constraint of the acceleration about each body axis, an absolute rate limit, an angular momentum zonotope spanned by reaction wheels, or an angular momentum ellipsoid resulting from control moment gyroscopes (CMGs). If this holds, given a start attitude and rotation rate $(\boldsymbol{\Psi}_1, \boldsymbol{\omega}_{\mathrm{s},1})$ and corresponding end attitude and rotation rate $(\boldsymbol{\Psi}_2, \boldsymbol{\omega}_{\mathrm{s},2})$, the slew duration can then be expressed as function $T_{\mathrm{slew},12} = S\left(\boldsymbol{\Psi}_1, \boldsymbol{\omega}_{\mathrm{s},1}, \boldsymbol{\Psi}_2, \boldsymbol{\omega}_{\mathrm{s},2}\right)$. Moreover, the following relation must hold:

$$\boldsymbol{\Psi}_1^\intercal \boldsymbol{\Psi}_2 = \boldsymbol{\Psi}_3^\intercal \boldsymbol{\Psi}_4 \wedge \boldsymbol{\omega}_{\mathrm{s},1} = \boldsymbol{\omega}_{\mathrm{s},3} \wedge \boldsymbol{\omega}_{\mathrm{s},2} = \boldsymbol{\omega}_{\mathrm{s},4} \implies T_{\mathrm{slew},12} = T_{\mathrm{slew},34} \tag{1}$$

with all angular velocities expressed in body frame. If non-inertial constraints, for example limited rotation rates with respect to Earth-fixed reference or inertial constraints expressed in inertial frame, for example exclusion zones in the attitude space, are included, Equation 1 does not hold.

Even if a function S which is directly mapping the boundary conditions to a slew duration, is found, the problem is still inherently recursive, which can be seen in Figure 2. The shaded region marks the recursion. The slew duration obviously depends on the boundary conditions given by f, but the input to f also depends on the slew duration since the satellite itself is moving during the slew and to a lesser extend, so is the target point. Guaranteeing the validity of the resulting trajectory usually involves numerically checking the whole time series. This – in combination with the iterative nature of trajectory optimization – leads to excessive run time.

The slew duration must be calculated as accurately as possible. Consider a scenario where the satellite has just finished observing a target far away in along-track direction and is then tasked to switch to another target, also in along-track direction. While the targets are far away, the apparent angle between them as seen from the satellite is small, as illustrated in Figure 3. It is a sensible assumption that the size of this apparent angle positively correlates with the slew duration. Therefore, the slew duration tends to be shorter. If the slew duration is underestimated, the next targets are assumed to be further away, leading to assumed shorter slew duration, which not only leads to an accumulation of errors, but also degrades all next estimations. Vice-versa, the same applies. If the slew duration is overestimated, the assumed apparent angle between targets increases more than it should, leading again to longer assumed slew durations for the next estimations. We conclude that the slew duration must be calculated as accurately as feasibly possible to avoid these problems entirely.

DOI: 10.13009/EUCASS2025-378

3. Minimal Parametrization of Observation Targets

3.1 Geometric Parametrization for Non-Rotating Earth

As established earlier, the required attitude and angular rate to observe a target can be determined by its position, velocity, a target location on Earth, and the requested scan direction for the target. In total, this sums up to 10 parameters. To calculate the duration of a slew from one target to the next, the parametrization must contain information about the position and direction of the second target. Therefore, 14 parameters are sufficient to fully describe the boundary conditions of the slew in the context of a given satellite under the previously established assumptions, which gives an upper bound for the number of dimensions needed.

The goal is now to reduce the number of parameters as much as possible, so the whole parameter-space can be sampled and each corresponding value for the slew duration stored in a lookup-table. For efficient interpolation between samples, the distribution of data points should fulfill the following requirements. First, it is desirable that a uniform sampling distance in the parameter space translates into a uniform distribution of targets on ground. Second, the distribution must be orthogonal through all dimensions for applicability of quick interpolation algorithms.

As first step, the problem is simplified by assuming a circular orbit and spherical Earth. For now, we neglect the Earth's rotation, which we will reintroduce and compensate in subsection 3.2. Given the reference orbit of a spacecraft, it is possible to fully describe a point $\boldsymbol{p}_\mathrm{t}$ on Earth using the time where the line-of-sight from the spacecraft to $\boldsymbol{p}_\mathrm{t}$ is perpendicular to its velocity vector and the angular deviation from nadir η_PE necessary for the spacecraft to point at $\boldsymbol{p}_\mathrm{t}$. All vectors are given in an Earth-centered inertial (ECI) frame. We call this the perpendicular encounter (PE). Formally, a time of PE are all t_PE, for which the following conditions hold:

$$\left(\boldsymbol{p}_\mathrm{t}\left(t_\mathrm{PE}\right) - \boldsymbol{p}_\mathrm{s}\left(t_\mathrm{PE}\right)\right)^\intercal \boldsymbol{v}_\mathrm{s}\left(t_\mathrm{PE}\right) = 0 \tag{2}$$

$$\left(\boldsymbol{p}_\mathrm{s}\left(t_\mathrm{PE}\right) - \boldsymbol{p}_\mathrm{t}\left(t_\mathrm{PE}\right)\right)^\intercal \boldsymbol{p}_\mathrm{t}\left(t_\mathrm{PE}\right) > 0 \tag{3}$$

The first condition makes sure that the line-of-sight to the target is perpendicular to the velocity vector, the second condition ensures direct line of sight between satellite and target. Given the orbit and target position as time series in an ECI frame, typically several solutions for t_PE can be found, each representing a separate pass with an opportunity to observe the target. For each of these opportunities, the off-nadir angle η_PE at the time of perpendicular encounter can be calculated:

$$\eta_\mathrm{PE} = \arcsin\left(\frac{\left(\boldsymbol{p}_\mathrm{t}\left(t_\mathrm{PE}\right) - \boldsymbol{p}_\mathrm{s}\left(t_\mathrm{PE}\right)\right)^\intercal}{\left\|\boldsymbol{p}_\mathrm{t}\left(t_\mathrm{PE}\right) - \boldsymbol{p}_\mathrm{s}\left(t_\mathrm{PE}\right)\right\|}\left(\frac{\boldsymbol{p}_\mathrm{s}\left(t_\mathrm{PE}\right)}{h + R_\mathrm{E}} \times \frac{\boldsymbol{v}_\mathrm{s}\left(t_\mathrm{PE}\right)}{\left\|\boldsymbol{v}_\mathrm{s}\left(t_\mathrm{PE}\right)\right\|}\right)\right) \tag{4}$$

Given η_PE and t_PE, it must be possible to obtain $\boldsymbol{p}_\mathrm{t}$ iff the parametrization is bijective. In the following, the inverse transformation corresponding to equation Equation 4 is derived. The idea is to rotate the nadir-pointing line-of-sight vector $\left(\boldsymbol{p}_\mathrm{g} - \boldsymbol{p}_\mathrm{s}\right)$ about the velocity vector $\boldsymbol{v}_\mathrm{s}$ by the angle η_PE and scaling it by D/h with orbital altitude h and slant distance[13] D:

$$D(\eta) = (h + R_\mathrm{E})\cos\eta - \sqrt{R_\mathrm{E}^2 - (h + R_\mathrm{E})^2 \sin^2\eta} \tag{5}$$

For brevity, the argument t_PE is omitted for $\boldsymbol{p}_\mathrm{t}$, $\boldsymbol{p}_\mathrm{s}$, $\boldsymbol{p}_\mathrm{g}$ and $\boldsymbol{v}_\mathrm{s}$. With $\mathbb{1}$ denoting the 3×3 unit matrix we can write

$$\boldsymbol{R}\left(\boldsymbol{v}, \alpha\right) := \left[\boldsymbol{v}\times\right]\sin\alpha + \mathbb{1}\cos\alpha + \boldsymbol{v}\boldsymbol{v}^\intercal\left(1 - \cos\alpha\right) \tag{6}$$

where $\left[\boldsymbol{v}\times\right] \in \mathrm{SO}(3)$ is the skew symmetric matrix of $\boldsymbol{v} \in \mathbb{R}^3$ such that $\left[\boldsymbol{v}\times\right]\boldsymbol{w} = \boldsymbol{v} \times \boldsymbol{w}$. Inserting the rotation axis $\hat{\boldsymbol{v}}_\mathrm{s} = \boldsymbol{v}_\mathrm{s}/\left\|\boldsymbol{v}_\mathrm{s}\right\|$ and angle η_PE into Equation 6, we can write

$$\boldsymbol{p}_\mathrm{t} - \boldsymbol{p}_\mathrm{s} = \frac{D}{h}\boldsymbol{R}\left(\hat{\boldsymbol{v}}_\mathrm{s}, \eta_\mathrm{PE}\right)\left(\boldsymbol{p}_\mathrm{g} - \boldsymbol{p}_\mathrm{s}\right) \tag{7}$$

Substituting for $\boldsymbol{R}\left(\boldsymbol{v}, \alpha\right)$ yields

$$\boldsymbol{p}_\mathrm{t} - \boldsymbol{p}_\mathrm{s} = \frac{D}{h}\left(\sin\eta_\mathrm{PE}\left[\hat{\boldsymbol{v}}_\mathrm{s}\times\right] + \mathbb{1}\cos\left(\eta_\mathrm{PE}\right) + \hat{\boldsymbol{v}}_\mathrm{s}\hat{\boldsymbol{v}}_\mathrm{s}^\intercal\left(1 - \cos\left(\eta_\mathrm{PE}\right)\right)\right)\left(\boldsymbol{p}_\mathrm{g} - \boldsymbol{p}_\mathrm{s}\right) \tag{8}$$

$$= \frac{D}{h}\left(\sin\eta_\mathrm{PE}\left[\hat{\boldsymbol{v}}_\mathrm{s}\times\right] + \mathbb{1}\sqrt{1 - \left(\sin\eta_\mathrm{PE}\right)^2} + \hat{\boldsymbol{v}}_\mathrm{s}\hat{\boldsymbol{v}}_\mathrm{s}^\intercal\left(1 - \sqrt{1 - \left(\sin\eta_\mathrm{PE}\right)^2}\right)\right)\left(\boldsymbol{p}_\mathrm{g} - \boldsymbol{p}_\mathrm{s}\right) \tag{9}$$

DOI: 10.13009/EUCASS2025-378

where we used the fact that $\eta_{\mathrm{PE}} < 90°$. Substituting $\left(\boldsymbol{p}_{\mathrm{g}} - \boldsymbol{p}_{\mathrm{s}}\right) = -h/\left(h + R_{\mathrm{E}}\right)\boldsymbol{p}_{\mathrm{s}}$ and $\hat{\boldsymbol{v}}_{\mathrm{s}}^{\mathrm{T}}\boldsymbol{p}_{\mathrm{s}} = 0$ yields

$$\boldsymbol{p}_{\mathrm{t}} - \boldsymbol{p}_{\mathrm{s}} = -\frac{D}{h + R_{\mathrm{E}}}\left(\sin\eta_{\mathrm{PE}}\hat{\boldsymbol{v}} \times \boldsymbol{p}_{\mathrm{s}} + \sqrt{1 - (\sin\eta_{\mathrm{PE}})^2}\boldsymbol{p}_{\mathrm{s}}\right) \tag{10}$$

and with one final rearrangement

$$\boldsymbol{p}_{\mathrm{t}} = \boldsymbol{p}_{\mathrm{s}} - \frac{D\left(\eta_{\mathrm{PE}}\right)}{h + R_{\mathrm{E}}}\left(\sin\eta_{\mathrm{PE}}\hat{\boldsymbol{v}} \times \boldsymbol{p}_{\mathrm{s}}\left(t_{\mathrm{PE}}\right) + \sqrt{1 - (\sin\eta_{\mathrm{PE}})^2}\boldsymbol{p}_{\mathrm{s}}\left(t_{\mathrm{PE}}\right)\right). \tag{11}$$

In Appendix A, we insert Equation 4 into Equation 11 and show that there is no contradiction. The remaining degree of freedom is the direction of the target A, which is already only a single parameter. We have therefore reduced the problem to three parameters per target.

Additionally, for the calculations below and to facilitate visualizing the problem, alternative equivalent parameters are introduced based on the geometric relations described by Wertz et al[13]:

$$|\lambda| = \arcsin\left(\frac{h + R_{\mathrm{E}}}{R_{\mathrm{E}}}\sin|\eta|\right) - |\eta| \tag{12}$$

Since $\sin(-x) = -\sin(x)$ and $\arcsin(-x) = -\arcsin(x)$ directional information can be retained. Additionally, we define λ negative with respect to η to achieve the same handedness of rotations with respect to a given rotation axis, for example the flight direction:

$$\lambda = \eta - \arcsin\left(\frac{h + R_{\mathrm{E}}}{R_{\mathrm{E}}}\sin\eta\right) \tag{13}$$

Similarly, the inverse transformation is then

$$\tan\eta = -\frac{\sin\rho\sin\lambda}{1 - \sin\rho\cos\lambda} \tag{14}$$

with $\sin\rho = \frac{R_{\mathrm{E}}}{R_{\mathrm{E}}+h}$.

Similarly for t_{PE}, the equivalent difference in argument of latitude u can be defined:

$$\Delta u = \Delta t_{\mathrm{PE}}\omega_{\mathrm{orb}} \tag{15}$$

with ω_{orb} being the orbital rate of the satellite.

Assuming non-rotating Earth, it is guaranteed that the geometric relationship between the satellite and $\boldsymbol{p}_{\mathrm{t}}$ expressed in the orbital frame is always the same, regardless of the absolute time reference and thus argument of latitude. In Figure 4, one can see that this holds, as long as both λ and the along-track distance of the targets remain constant. The equator and poles are not shown since they are not relevant to the geometry in the static case. To uniquely determine the geometric relation between the satellite and the two targets, only the relative timings are necessary. As time reference, the start of the slew is defined as $t = 0$. t_{PE} for either target is then expressed relative to this. Since the boundary conditions can be computed from $\lambda_{\mathrm{PE},1}, t_{\mathrm{PE},1}, A_1, \lambda_{\mathrm{PE},2}, t_{\mathrm{PE},2}, A_2$, all necessary information can be recovered. Ideally, it is then possible to find the time optimal slew, automatically fulfilling Equation 1. If only approximately optimal methods are applied, as for example shown by Barschke et al[3], it must be ensured that Equation 1 is fulfilled. Due to the comparatively low number of dimensions involved, we suggest precomputing a look-up table (LuT) with this accurate but slow method, combining high accuracy with fast table lookup. For the ideal case that Earth does not spin, the LuT then directly contains the true slew duration.

3.2 Consideration of Earth's Rotation

Considering Earth's rotation simply means reintroducing the time dependency of $\boldsymbol{p}_{\mathrm{t}}$. As a first order approximation, the movement of $\boldsymbol{p}_{\mathrm{t}}$ can be modeled as constant rotation about Earth's axis with constant angular rate ω_{E} (rotation rate of Earth). Consequentially, the geometric relationship between the satellite and $\boldsymbol{p}_{\mathrm{t}}$ is now no longer independent from the absolute location, as both the magnitude and direction of rotating Earth as seen from the satellite is depending on the latitude of the target and α, denoting the angle between the ground track and the circle of latitude at the sub-satellite-point. Since all these are known quantities, one can compensate for this movement and analytically extrapolate how a

DOI: 10.13009/EUCASS2025-378

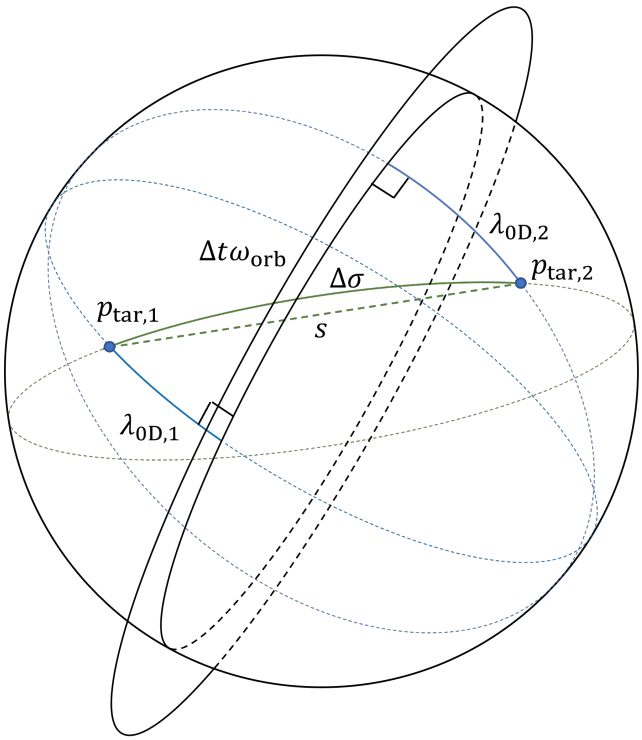

Figure 4: Relative geometry of orbit and two observations

target point moves through the field of view of the satellite expressed in terms of above parameters. Only if $t = t_{\text{PE}}$, the parameters are the same as in the non-rotating case. In Figure 5, an enlarged representation of the geometric relations between the satellite and target at $t = t_{\text{PE}}$ and $t = t_{\text{PE}} + \Delta t$ is shown. One can observe, the distance between the instantaneous line of nodes and the circle of longitude is increasing by $\Delta t\omega_{\text{E}}$, resulting in a change of the relative observation parameters. Spherical trigonometry is used to derive this relation, so we give a brief overview here.

The relevant equations (Napier's rules) from spherical trigonometry for right spherical triangles with a triangle where A, B, C are the surface angles and a, b, c the central angles (or edges) with $C = 90°$ as shown in Figure 6 are the following[12]:

$$\cos c = \cos a \cos b \tag{16a}$$
$$\sin a = \sin A \sin c \tag{16b}$$
$$\tan a = \tan A \sin b \tag{16c}$$
$$\tan b = \tan B \sin a \tag{16d}$$
$$\tan b = \cos A \tan c \tag{16e}$$

In Figure 5, two pairs (colored blue and green) of spherical triangles are depicted, where in each pair there is one triangle with the edges (λ, x, u) and one with the edges $(\Delta\Omega, x', \Phi)$. Given t_{PE}, the argument of latitude u is obtained from the sub-satellite point $\boldsymbol{p}_{\text{g}}$ at the time. In the following, λ_{PE} is for brevity called λ. Using Equation 16a on the upper blue triangle yields:

$$\cos x = \cos\lambda \cos u \tag{17}$$

Similarly, again using Equation 16a on the lower blue triangle yields:

$$\cos\Delta\Omega = \frac{\cos x}{\cos\Phi} = \frac{\cos\lambda\cos u}{\cos\Phi} \tag{18}$$

Optionally, Equation 16c and Equation 16d can be used on the upper and lower triangle to obtain β and α, which gives

DOI: 10.13009/EUCASS2025-378

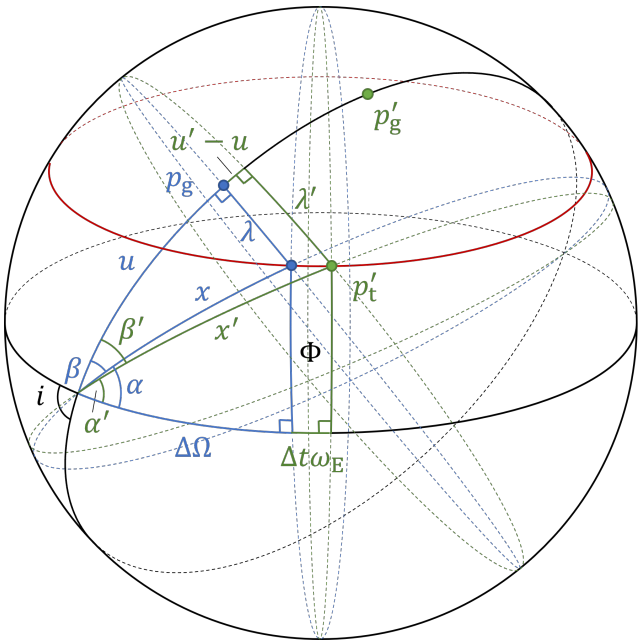

Figure 5: Spherical trigonometric relations to account for Earth's rotation

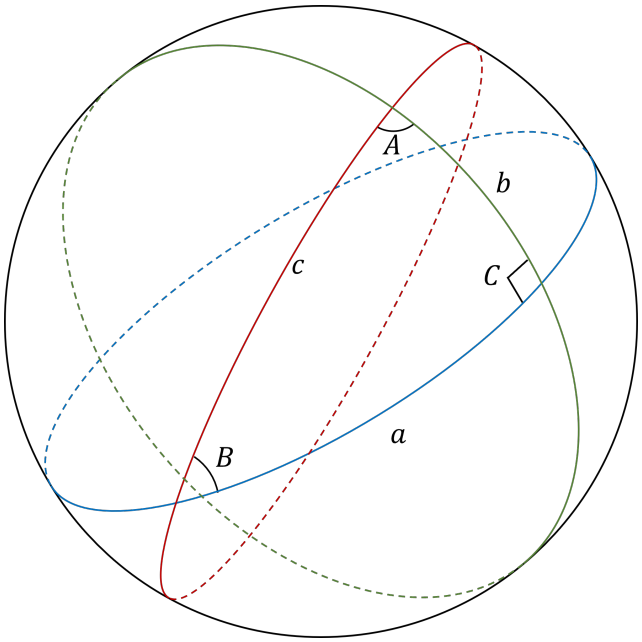

Figure 6: Triangle on a sphere

a way to obtain the orbit's inclination i if it is not known otherwise beforehand:

$$\tan\beta = \frac{\tan\lambda}{\sin u} \tag{19}$$

$$\tan\alpha = \frac{\tan\Phi}{\sin\Delta\Omega} \tag{20}$$

$$i = \alpha + \beta \tag{21}$$

Then, the instantaneous line of nodes is incremented by $\Delta t\omega_E$ while the latitude Φ is constant, enabling calculation of x' using Equation 16a on the lower green triangle:

$$\cos x' = \cos\left(\Delta\Omega + \Delta t\omega_E\right)\cos\Phi \tag{22}$$

DOI: 10.13009/EUCASS2025-378

Additionally, α' is calculated using Equation 16d, and using Equation 21 yields β':

$$\tan\alpha' = \frac{\tan\Phi}{\sin\left(\Delta\Omega + \Delta t\omega_{\mathrm{E}}\right)} \tag{23}$$

$$\beta' = i - \alpha' \tag{24}$$

Since two angles of the upper green triangle (and the right angle) are now known, Equation 16b and Equation 16e can be used to obtain λ' and u', respectively:

$$\sin\lambda' = \sin\beta' \sin x' \tag{25}$$

$$\tan u' = \cos\beta' \tan x' \tag{26}$$

Then, one can use Equation 14 to obtain η'_{PE} and Equation 15 to obtain t'_{PE}:

$$t'_{\mathrm{PE}} = t_{\mathrm{PE}} + \frac{u' - u}{\omega_{\mathrm{orb}}} \tag{27}$$

Caution is advised when implementing these equations, as case discriminations are necessary when for example $\Delta\Omega + \Delta t\omega_{\mathrm{E}}$ switches sign or passes trough 90° to avoid trigonometric ambiguities. Equations 25-27 thus specify the perpendicular encounter (PE) parameters for the target after compensating for Earth's rotation.

Given a pair of targets, the compensated parameters for the first target can be obtained immediately given $t_{\mathrm{PE},1}$ and $\eta_{\mathrm{PE},1}$. Similar to the original problem shown in Figure 2, the solution for the second target must be found iteratively, since the time of observation depends on the slew duration itself. However, now the bottleneck of computing the full slew and checking for constraint violations is replaced by a quick table-lookup.

4. Numerical Verification

4.1 Test Setup

We now apply the PE parametrization to compute slew durations between randomly selected pairs of observations using only the pair's PE parametrization. As a baseline, we use a method similar to the one described by Barschke et al[3] to provide "truth" values for the slew durations. We expect that using the PE parameters allows to compute the times with sufficient accuracy but lower computational effort. The test case is a single satellite in circular orbit with an altitude of 500 km and 80° inclination. Taking an observation at $\boldsymbol{p}_{\mathrm{t}}$ with scan direction $\hat{e}_{\mathrm{scan}}$ while the satellite is at $\boldsymbol{p}_{\mathrm{s}}$ fixes the attitude as follows:

$$\hat{\boldsymbol{e}}_z = \frac{\boldsymbol{p}_{\mathrm{t}} - \boldsymbol{p}_{\mathrm{s}}}{\left\|\boldsymbol{p}_{\mathrm{t}} - \boldsymbol{p}_{\mathrm{s}}\right\|} \tag{28}$$

$$\hat{\boldsymbol{e}}_y = \hat{\boldsymbol{e}}_z \times \hat{\boldsymbol{e}}_{\mathrm{scan}} \tag{29}$$

$$\hat{\boldsymbol{e}}_x = \hat{\boldsymbol{e}}_y \times \hat{\boldsymbol{e}}_z \tag{30}$$

$$\boldsymbol{R}_{\mathrm{BI}} = \begin{bmatrix}\hat{\boldsymbol{e}}_x & \hat{\boldsymbol{e}}_y & \hat{\boldsymbol{e}}_z\end{bmatrix} \tag{31}$$

The scan direction vector $\hat{e}_{\mathrm{scan}}$ can be computed based on an absolute scan azimuth A_{scan}:

$$\hat{\boldsymbol{e}}_{\mathrm{east}} = \begin{bmatrix}0 & 0 & 1\end{bmatrix}^{\mathsf{T}} \times \frac{\boldsymbol{p}_{\mathrm{t}}}{R_{\mathrm{E}}} \tag{32}$$

$$\hat{\boldsymbol{e}}_{\mathrm{north}} = \frac{\boldsymbol{p}_{\mathrm{t}}}{R_{\mathrm{E}}} \times \hat{\boldsymbol{e}}_{\mathrm{east}} \tag{33}$$

$$\hat{\boldsymbol{e}}_{\mathrm{scan}} = \hat{\boldsymbol{e}}_{\mathrm{north}} \cos A_{\mathrm{scan}} + \hat{\boldsymbol{e}}_{\mathrm{east}} \sin A_{\mathrm{scan}} \tag{34}$$

For the rotation rate of the spacecraft $\boldsymbol{\omega}_{\mathrm{s}}$, it is assumed that the spacecraft continues looking on the same spot of the Earth with the same scan direction (equivalent to a staring array). For the first test, each scan is assumed to be performed with the scan direction aligned with the satellite's instantaneous velocity vector.

If the satellite is performing a slew, the boundary conditions for the first observation are fixed, since the start time of the slew is already known. The underlying assumption is that it is always best to start the slew immediately. To determine the minimal slew duration, candidate solutions are iterated and fed into a trajectory optimization[3] which uses polynomial profiles for the attitude. The only constraint is a maximum rotation rate of 3 °/s in each body axis.

DOI: 10.13009/EUCASS2025-378

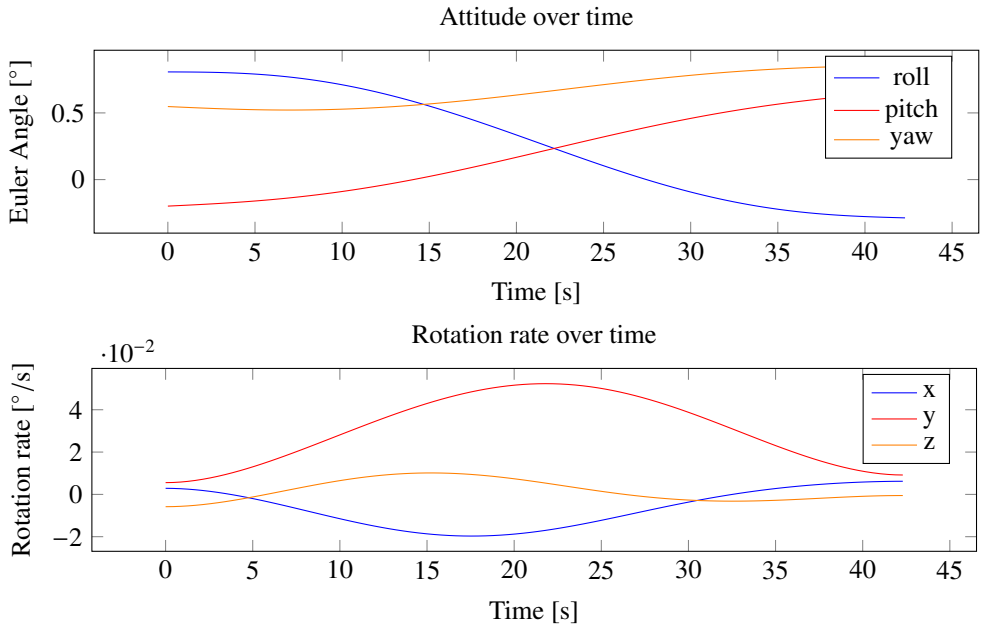

Figure 7: Non-rest to non-rest slew guidance example

The acceleration and jerk are guaranteed to be bounded due to the inherent smoothness and differentiability of the underlying polynomial guidance, which also limits the torque. The polynomial slew interpolation, which is originally performed in the rotating orbital reference frame, is adapted to be performed with respect to a non-rotating orbital reference frame, fixed at the start of the slew. This is necessary to guarantee fulfillment of Equation 1. An example of a resulting slew is shown in Figure 7.

We further assume that the satellite cannot perform observations with an off-nadir angle larger than 45°. Since this constraint can easily be incorporated afterwards by defining earliest start and latest end times of observations and checking against the predicted slew duration, it is not considered in the calculation of the slew duration itself. It only serves as minimum and maximum value for η_{PE} when generating the LuT and looking up values. The maximum separation in time is assumed to be 100 s, meaning $-100\,\mathrm{s} < t_{\mathrm{PE}} < 100\,\mathrm{s}$ for either target. Since the Azimuth is fixed parallel to the ground track for every observation, it does not need to be sampled separately. The LuTs therefore only have four dimensions, $t_{\mathrm{PE},1}, t_{\mathrm{PE},2}, \eta_{\mathrm{PE},1}$ and $\eta_{\mathrm{PE},2}$.

4.2 Results

With the model and constraints described above, two LuTs are generated, one with 25 data points per axis, the other with 49. The tables are generated based on the ideal model with non-rotating Earth, since this is compensated later. The resulting maximum slew duration in the data sets is 76.65 s. Using table interpolation, one sample with specified values for $(t_{\mathrm{PE},1}, t_{\mathrm{PE},2}, \eta_{\mathrm{PE},1}, \eta_{\mathrm{PE},2})$ can be looked up. At the same time, the true slew duration is determined based on the model described in subsection 4.1, so the error can be calculated as the difference between the value obtained from the LuT and the ground truth. Three configurations are tested with 10 000 randomly selected samples of observation pairs each:

1. Ideal case: Earth is not rotating
2. Rotating Earth but no compensation used
3. Rotating Earth which is compensated using method described in subsection 3.2

In Figure 8a and 8b, the results for the ideal case are shown. One can clearly see that there is no dependency on the argument of latitude. The main source of error is the interpolation between data points. It gets smaller with higher resolution, as can be seen both in Table 1 and Figure 9.

In Figure 8c and 8d, the results for the second case are shown. In both cases the error is much larger than in the ideal case. This is expected, now $\omega_{\mathrm{E}} \neq 0$ and it has a much larger impact at the equator due to the larger distance of the target to the rotation axis. In both latitude variations the slew duration appears to be slightly overestimated. This is

DOI: 10.13009/EUCASS2025-378

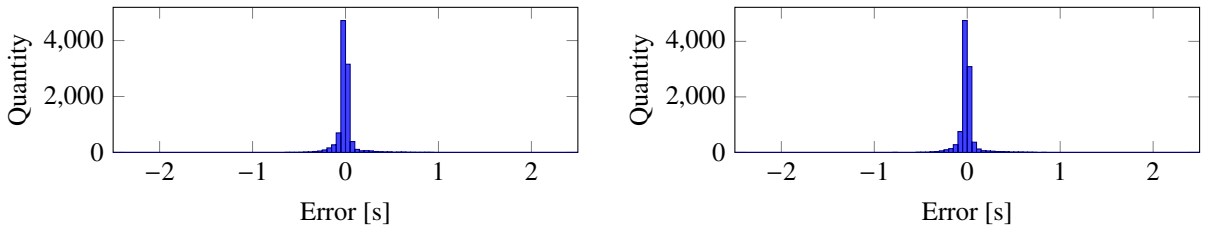

(a) Ideal case, $u = 90°$

(b) Ideal case, $u = 180°$

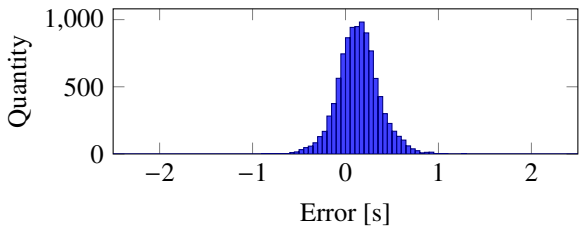

(c) Earth rotating (uncompensated), $u = 90°$

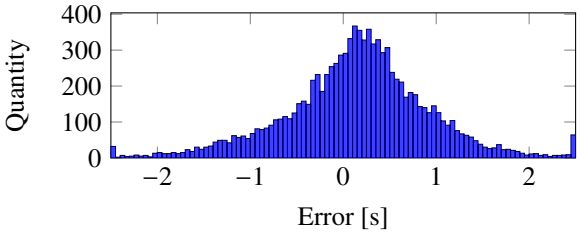

(d) Earth rotating (uncompensated), $u = 180°$

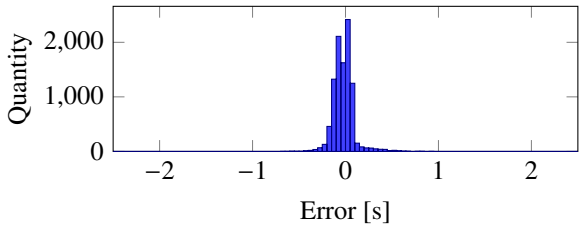

(e) Earth rotating (compensated), $u = 90°$

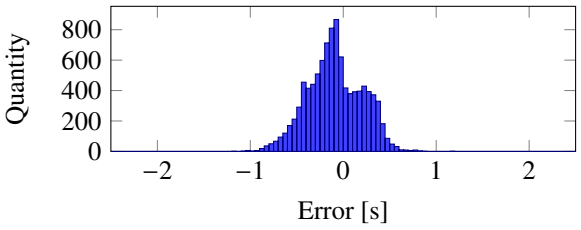

(f) Earth rotating (compensated), $u = 180°$

Figure 8: Histograms of slew duration estimation error

also expected, since the inclination is below 90°, the Earth rotates with the orbit and the along-track component of the target's apparent velocity is positive.

In Figure 8e and 8f, the results for the third case are shown. The compensation reduces the error again to acceptable values. We still see a larger error at the equator than at the pole. The apparent movement of the target not only impacts the absolute attitude or pointing of the satellite, but also the rotation rate of the spacecraft at the beginning and end of a slew. This movement is more significant at the equator, the remaining uncompensated deviation is therefore larger. The compensation only addresses the attitude and not the rate. In Figure 9, one can see that increasing the number of samples in the LuT does affect the accuracy in the ideal case. In the compensated case there is no significant difference, at least not in the more critical equator scenario. Since increasing the size of the LuT comes at the cost of higher memory usage and longer lookup time, the version with lower resolution is preferable.

Table 1: Slew duration estimation error

Case	**LuT size**	**Percentile error [s]**				
		50 %	90 %	99 %	99.9 %	Max
ideal, pole	$25^4 = 390\,625$	0.0216	0.1040	0.3862	0.6825	0.9369
ideal, equator		0.0224	0.1032	0.3886	0.6873	0.8069
uncompensated, pole		0.1725	0.4294	0.7024	0.9170	1.2988
uncompensated, equator		0.4549	1.2968	2.4263	3.5467	4.3684
compensated, pole		0.0613	0.1577	0.4192	0.6361	0.9481
compensated, equator		0.2164	0.4839	0.7764	0.9921	1.1885
ideal, pole	$49^4 = 5\,764\,801$	0.0161	0.0437	0.1643	0.3365	0.4566
ideal, equator		0.0168	0.0466	0.1723	0.3707	0.4612
compensated, pole		0.0534	0.1249	0.2083	0.3341	0.4355
compensated, equator		0.2045	0.4693	0.7559	0.8988	1.0705

DOI: 10.13009/EUCASS2025-378

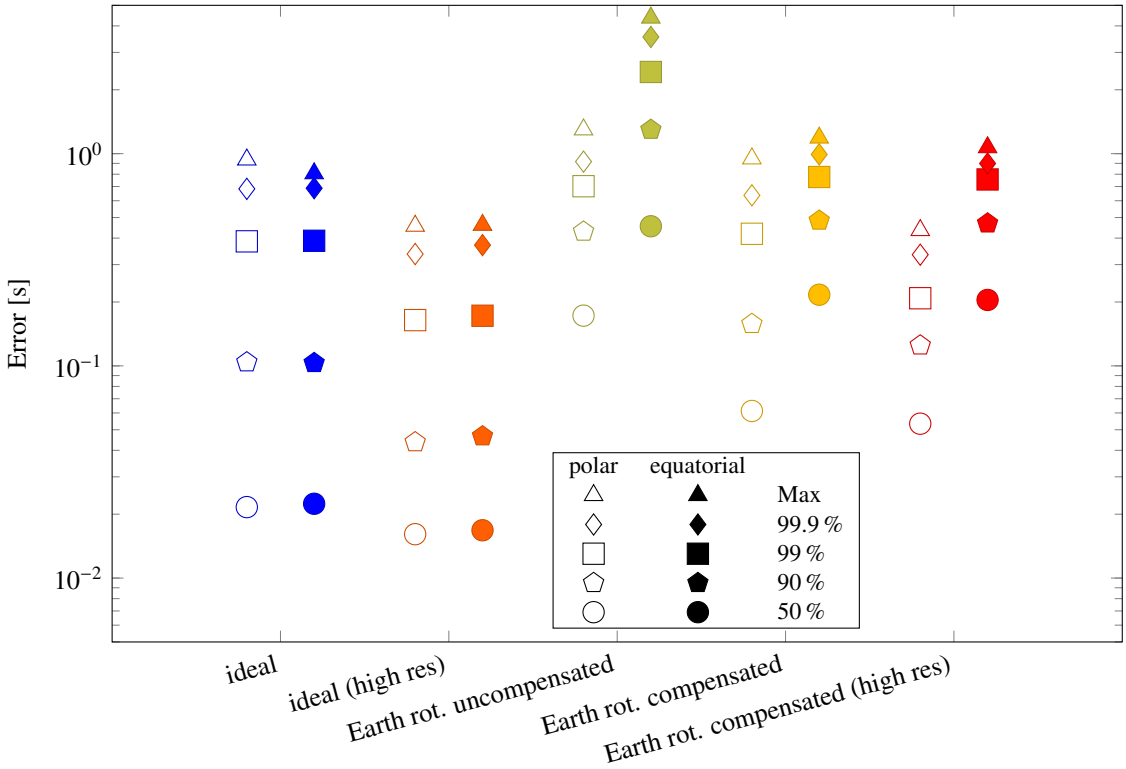

Figure 9: Slew duration estimation error

5. Conclusion

This paper presents two advancements for the agile earth observation system (EOS) planning problem. First, we have presented a novel, general and minimal parametrization of observation targets applicable to a wide range of EOS, including staring arrays, time delay integration (TDI) type optical instruments and radar antennas. We show that this parametrization contains all required information to compute slew durations. It replaces a time and resource consuming part of optimal planning by much cheaper table lookup. Second, an implementation of the above concepts is demonstrated, showing both the applicability and adequacy of look-up tables (LuTs) for calculating the duration of agile non-rest to non-rest slews. As a result, the simplicity and scalability of LuTs is combined with high-fidelity attitude models. This method could also be used to train reinforcement learning agents as presented by Stephenson et al[11], improving the quality of the training environment resulting in better informed decisions. In the future, more compensation methods can be developed, for example considering eccentric orbits, non-spherical Earth, varying the target altitude or incorporating the difference in angular rate of the spacecraft when observing targets at different latitudes, further enhancing the accuracy while retaining low dimensionality and quick runtime.

References

[1] Johannes Aldinger and Johannes Löhr. “Planning for Agile Earth Observation Satellites”. In: *Proceedings of the ICAPS-2013 Workshop on Planning in Continuous Domains (PCD)*. 2013.

[2] Sean Augenstein et al. “Optimal Scheduling of a Constellation of Earth-Imaging Satellites, for Maximal Data Throughput and Efficient Human Management”. In: 2016.

[3] Merlin F. Barschke et al. “ASSET: a software tool for the evaluation of manoeuvre capabilities of highly agile satellites”. In: *CEAS Space Journal* 6.1 (Mar. 2014), pp. 37–45. DOI: 10.1007/s12567-013-0057-2.

[4] Virginie Gabrel et al. “A new single model and derived algorithms for the satellite shot planning problem using graph theory concepts”. In: *Annals of Operations Research - Annals OR* 69 (Jan. 1997), pp. 115–134. DOI: 10.1023/A:1018920709696.

[5] Romain Grasset-Bourdel, Gérard Verfaillie, and Antoine Flipo. “Action and Motion Planning for Agile Earth-Observing Satellites”. In: *Acta Futura 5*. 2012, pp. 121–131.

DOI: 10.13009/EUCASS2025-378

[6] Nicholas G. Hall and Michael J. Magazine. "Maximizing the value of a space mission". In: *European Journal of Operational Research* 78.2 (1994), pp. 224–241. ISSN: 0377-2217. DOI: https://doi.org/10.1016/0377-2217(94)90385-9. URL: https://www.sciencedirect.com/science/article/pii/0377221794903859.

[7] A. Herrmann and H. Schaub. "A Comparison Of Deep Reinforcement Learning Algorithms For Earth-Observing Satellite Scheduling". In: *AAS/AIAA Spaceflight Mechanics Meeting* (Jan. 2023).

[8] Michel Lemaître et al. "Selecting and scheduling observations of agile satellites". In: *Aerospace Science and Technology* 6 (Sept. 2002), pp. 367–381. DOI: 10.1016/S1270-9638(02)01173-2.

[9] Sreeja Nag, Alan S. Li, and James H. Merrick. "Scheduling algorithms for rapid imaging using agile Cubesat constellations". In: *Advances in Space Research* 61.3 (2018), pp. 891–913. ISSN: 0273-1177. DOI: https://doi.org/10.1016/j.asr.2017.11.010. URL: https://www.sciencedirect.com/science/article/pii/S0273117717308050.

[10] Mark Stephenson and Hanspeter Schaub. "Optimal Target Sequencing in the Agile Earth-Observing Satellite Scheduling Problem using Learned Dynamics". In: *AAS/AIAA Astrodynamics Specialist Conference* (Aug. 2023).

[11] Mark Stephenson and Hanspeter Schaub. "Reinforcement Learning for Earth-Observing Satellite Autonomy with Event-Based Task Intervals". In: *AAS/AIAA Astrodynamics Specialist Conference* (Feb. 2024).

[12] I. Todhunter. *Spherical Trigonometry, for the Use of Colleges and Schools: With Numerous Examples*. Project Gutenberg, Aug. 2020, p. 39. URL: https://www.gutenberg.org/files/19770/19770-pdf.pdf.

[13] J.R. Wertz and W.J. Larson. *Space Mission Analysis and Design*. Space Technology Library. Springer, 1991, p. 113. ISBN: 9780792309703.

[14] Xuexuan Zhao, Zhaokui Wang, and G.T. Zheng. "Two-Phase Neural Combinatorial Optimization with Reinforcement Learning for Agile Satellite Scheduling". In: *Journal of Aerospace Information Systems* 17 (Mar. 2020), pp. 1–12. DOI: 10.2514/1.I010754.

A. Consistency of Parametrization

Rewriting Equation 4, we know

$$\sin\eta_{\mathrm{PE}} = \frac{(\boldsymbol{p}_{\mathrm{t}} - \boldsymbol{p}_{\mathrm{s}})^{\intercal}}{\left\|\boldsymbol{p}_{\mathrm{t}} - \boldsymbol{p}_{\mathrm{s}}\right\|}\left(\frac{\boldsymbol{p}_{\mathrm{s}}}{h + R_{\mathrm{E}}} \times \hat{\boldsymbol{v}}_{\mathrm{s}}\right) \tag{35}$$

which is a triple product of the form $a^{\intercal}(b \times c)$. Squaring this yields the Gram determinant of the three vectors:

$$(a^{\intercal}(b\times c))\cdot(a^{\intercal}(b\times c)) = \det\begin{bmatrix} a^{\intercal}a & a^{\intercal}b & a^{\intercal}c \\ b^{\intercal}a & b^{\intercal}b & b^{\intercal}c \\ c^{\intercal}a & c^{\intercal}b & c^{\intercal}c \end{bmatrix} \tag{36}$$

$$\begin{aligned} &= a^{\intercal}a\cdot b^{\intercal}b\cdot c^{\intercal}c + a^{\intercal}b\cdot b^{\intercal}c\cdot c^{\intercal}a + a^{\intercal}c\cdot b^{\intercal}a\cdot c^{\intercal}b \\ &- a^{\intercal}c\cdot b^{\intercal}b\cdot c^{\intercal}a - a^{\intercal}b\cdot b^{\intercal}a\cdot c^{\intercal}c - a^{\intercal}a\cdot b^{\intercal}c\cdot c^{\intercal}b \end{aligned} \tag{37}$$

Since all vectors involved are unit vectors, all same-vector dot-products are 1. The vector c (velocity) is orthogonal to both a (LOS) and b (position), so their dot product is 0. The dot product is commutative. Therefore

$$\begin{aligned} (a^{\intercal}(b\times c))\cdot(a^{\intercal}(b\times c)) &= 1 + a^{\intercal}b\cdot 0\cdot 0 + 0\cdot b^{\intercal}a\cdot 0 \\ &\quad - 0\cdot 1\cdot 0 - a^{\intercal}b\cdot b^{\intercal}a\cdot 1 - 1\cdot 0\cdot 0 && (38)\\ &= 1 - a^{\intercal}b\cdot b^{\intercal}a && (39)\\ &= 1 - (a^{\intercal}b)^2 && (40) \end{aligned}$$

Inserting the original terms yields

$$(\sin\eta_{\mathrm{PE}})^2 = 1 - \left(\frac{(\boldsymbol{p}_{\mathrm{t}} - \boldsymbol{p}_{\mathrm{s}})^{\intercal}}{\left\|\boldsymbol{p}_{\mathrm{t}} - \boldsymbol{p}_{\mathrm{s}}\right\|}\,\frac{\boldsymbol{p}_{\mathrm{s}}}{h + R_{\mathrm{E}}}\right)^2 \tag{41}$$

DOI: 10.13009/EUCASS2025-378

Therefore:

$$\sqrt{1-(\sin\eta_{\mathrm{PE}})^2} = \sqrt{1-\left(1-\left(\frac{(\boldsymbol{p}_\mathrm{t}-\boldsymbol{p}_\mathrm{s})^\intercal}{\left\|\boldsymbol{p}_\mathrm{t}-\boldsymbol{p}_\mathrm{s}\right\|}\frac{\boldsymbol{p}_\mathrm{s}}{h+R_\mathrm{E}}\right)^2\right)} \tag{42}$$

$$= \left|\frac{(\boldsymbol{p}_\mathrm{t}-\boldsymbol{p}_\mathrm{s})^\intercal}{\left\|\boldsymbol{p}_\mathrm{t}-\boldsymbol{p}_\mathrm{s}\right\|}\frac{\boldsymbol{p}_\mathrm{s}}{h+R_\mathrm{E}}\right| \tag{43}$$

From Equation 3, we know that the inside of the absolute-value brackets is always negative, so we can substitute

$$\sqrt{1-(\sin\eta_{\mathrm{PE}})^2} = -\frac{(\boldsymbol{p}_\mathrm{t}-\boldsymbol{p}_\mathrm{s})^\intercal}{\left\|\boldsymbol{p}_\mathrm{t}-\boldsymbol{p}_\mathrm{s}\right\|}\frac{\boldsymbol{p}_\mathrm{s}}{h+R_\mathrm{E}} \tag{44}$$

Substituting Equation 41 and Equation 44 in Equation 10 yields

$$\boldsymbol{p}_\mathrm{t}-\boldsymbol{p}_\mathrm{s} = -\frac{D}{h+R_\mathrm{E}}\cdot\left(\left(\frac{(\boldsymbol{p}_\mathrm{t}-\boldsymbol{p}_\mathrm{s})^\intercal}{\left\|\boldsymbol{p}_\mathrm{t}-\boldsymbol{p}_\mathrm{s}\right\|}\left(\frac{\boldsymbol{p}_\mathrm{s}}{h+R_\mathrm{E}}\times\hat{\boldsymbol{v}}_\mathrm{s}\right)\right)\hat{\boldsymbol{v}}_\mathrm{s}\times\boldsymbol{p}_\mathrm{s} - \left(\frac{(\boldsymbol{p}_\mathrm{t}-\boldsymbol{p}_\mathrm{s})^\intercal}{\left\|\boldsymbol{p}_\mathrm{t}-\boldsymbol{p}_\mathrm{s}\right\|}\frac{\boldsymbol{p}_\mathrm{s}}{h+R_\mathrm{E}}\right)\cdot\boldsymbol{p}_\mathrm{s}\right) \tag{45}$$

Since $D = \left\|\boldsymbol{p}_\mathrm{t}-\boldsymbol{p}_\mathrm{s}\right\|$ we can write

$$\boldsymbol{p}_\mathrm{t}-\boldsymbol{p}_\mathrm{s} = -\left(\left((\boldsymbol{p}_\mathrm{t}-\boldsymbol{p}_\mathrm{s})^\intercal\left(\frac{\boldsymbol{p}_\mathrm{s}}{h+R_\mathrm{E}}\times\hat{\boldsymbol{v}}_\mathrm{s}\right)\right)\cdot\hat{\boldsymbol{v}}_\mathrm{s}\times\frac{\boldsymbol{p}_\mathrm{s}}{h+R_\mathrm{E}} - \left((\boldsymbol{p}_\mathrm{t}-\boldsymbol{p}_\mathrm{s})^\intercal\frac{\boldsymbol{p}_\mathrm{s}}{h+R_\mathrm{E}}\right)\cdot\frac{\boldsymbol{p}_\mathrm{s}}{h+R_\mathrm{E}}\right) \tag{46}$$

$$= \left(\left((\boldsymbol{p}_\mathrm{t}-\boldsymbol{p}_\mathrm{s})^\intercal\left(\frac{\boldsymbol{p}_\mathrm{s}}{h+R_\mathrm{E}}\times\hat{\boldsymbol{v}}_\mathrm{s}\right)\right)\cdot\frac{\boldsymbol{p}_\mathrm{s}}{h+R_\mathrm{E}}\times\hat{\boldsymbol{v}}_\mathrm{s} + \left((\boldsymbol{p}_\mathrm{t}-\boldsymbol{p}_\mathrm{s})^\intercal\frac{\boldsymbol{p}_\mathrm{s}}{h+R_\mathrm{E}}\right)\cdot\frac{\boldsymbol{p}_\mathrm{s}}{h+R_\mathrm{E}}\right) \tag{47}$$

The vectors $\frac{\boldsymbol{p}_\mathrm{s}}{h+R_\mathrm{E}}$, $\hat{\boldsymbol{v}}_\mathrm{s}$ and $\frac{\boldsymbol{p}_\mathrm{s}}{h+R_\mathrm{E}}\times\hat{\boldsymbol{v}}_\mathrm{s}$ form an orthonormal basis. Since any vector can be expressed as the sum of dot products of the vector with each basis vector, we can write

$$\begin{aligned}\boldsymbol{p}_\mathrm{t}-\boldsymbol{p}_\mathrm{s} = {} & (\boldsymbol{p}_\mathrm{t}-\boldsymbol{p}_\mathrm{s})^\intercal\frac{\boldsymbol{p}_\mathrm{s}}{h+R_\mathrm{E}}\cdot\frac{\boldsymbol{p}_\mathrm{s}}{h+R_\mathrm{E}} \\ & + (\boldsymbol{p}_\mathrm{t}-\boldsymbol{p}_\mathrm{s})^\intercal\hat{\boldsymbol{v}}_\mathrm{s}\cdot\hat{\boldsymbol{v}}_\mathrm{s} \\ & + (\boldsymbol{p}_\mathrm{t}-\boldsymbol{p}_\mathrm{s})^\intercal\left(\frac{\boldsymbol{p}_\mathrm{s}}{h+R_\mathrm{E}}\times\hat{\boldsymbol{v}}_\mathrm{s}\right)\cdot\left(\frac{\boldsymbol{p}_\mathrm{s}}{h+R_\mathrm{E}}\times\hat{\boldsymbol{v}}_\mathrm{s}\right)\end{aligned} \tag{48}$$

Since the target position relative to the satellite $\boldsymbol{p}_\mathrm{t}-\boldsymbol{p}_\mathrm{s}$ at PE is perpendicular to the velocity vector per definition, the second term vanishes:

$$\boldsymbol{p}_\mathrm{t}-\boldsymbol{p}_\mathrm{s} = (\boldsymbol{p}_\mathrm{t}-\boldsymbol{p}_\mathrm{s})^\intercal\frac{\boldsymbol{p}_\mathrm{s}}{h+R_\mathrm{E}}\cdot\frac{\boldsymbol{p}_\mathrm{s}}{h+R_\mathrm{E}} + (\boldsymbol{p}_\mathrm{t}-\boldsymbol{p}_\mathrm{s})^\intercal\left(\frac{\boldsymbol{p}_\mathrm{s}}{h+R_\mathrm{E}}\times\hat{\boldsymbol{v}}_\mathrm{s}\right)\cdot\left(\frac{\boldsymbol{p}_\mathrm{s}}{h+R_\mathrm{E}}\times\hat{\boldsymbol{v}}_\mathrm{s}\right) \tag{49}$$

Which is identical to Equation 47, so we showed that indeed both sides of Equation 10 are equal. □